

Continuous separation, with microfluidics, of the components of a ternary mixture: from vacuum to purge gas pervaporation

Iwona Ziemecka¹  · Benoît Haut¹ · Benoit Scheid¹

Received: 9 January 2017 / Accepted: 4 April 2017 / Published online: 18 April 2017
© Springer-Verlag Berlin Heidelberg 2017

Abstract The general objective of this paper is to investigate the separation, with microfluidics, of the components of a ternary mixture, when using vacuum or purge gas pervaporation. The ternary mixture considered is a mixture of methanol (MeOH), water (H₂O) and hydrogen peroxide (H₂O₂). In a previous work (Ziemecka in Lab Chip 15:504–511, 2015), we presented the proof of concept of a microfluidic device, which was able to partially separate MeOH from the other components of such a mixture, by using vacuum pervaporation. Here, our goal is to optimize the operation of this device, by considering vacuum pervaporation, but also purge gas pervaporation. First, we provide a mathematical model of the device. This model is used to discuss the influence of the operating parameters on the device operation. To apply this model to the considered mixture, we determined the MeOH and H₂O permeability coefficients of PDMS membranes prepared from different concentrations of the curing agent. The model is then successfully compared to experimental data. The model and the experiments show that high efficiencies can be reached for both vacuum and purge gas pervaporation, provided a fine-tuning of the operating parameters. For instance, a good efficiency of the vacuum pervaporation is reached at

high temperature and low pressure. For purge gas pervaporation, it is reached for low temperature and high pressure.

Keywords Hydrogen peroxide · Microfluidics · Ternary mixture · Separation · Membrane · Vacuum pervaporation · Purge gas pervaporation

1 Introduction

Hydrogen peroxide (H₂O₂) has both reducing and oxidizing properties and is used in a wide spectrum of applications ranging from cosmetic products to military technology. Hydrogen peroxide is widely used in industry for bleaching purposes (paper, tissues) and water treatment. It can also be used as a source of green energy because when H₂O₂ is used as a fuel, it decomposes into water and oxygen, i.e. products with no environmental impact. It is produced in very high concentration (up to 70 wt% in water) through the anthraquinone process. The problems of that way of preparation are effective quinone recycling and formation of by-products, which have to be disposed.

In recent years, a new high-yield process has been developed (Bloomfield and Dhaese 2013) based on an optimized distribution of anthraquinone isomers for the production of solutions with 100% H₂O₂ content. This new process led to the construction of mega-scale plants able to produce massive amount of H₂O₂ per year, which should direct towards reductions in production costs. Nevertheless, another issue needing to be addressed lies on the fact that the manufacture of concentrated H₂O₂ cannot be performed where it is meant to be used. Indeed, the H₂O₂ production plants require specific authorization and are usually far from urban centres. Therefore, in most cases, dilution before transportation is needed.

✉ Iwona Ziemecka
Iwona.Ziemecka@ulb.ac.be

Benoît Haut
bhaut@ulb.ac.be

Benoit Scheid
bscheid@ulb.ac.be

¹ TIPs - Fluid Physics, Ecole polytechnique de Bruxelles, Université libre de Bruxelles, C.P. 165/67, avenue F.D. Roosevelt 50, 1050 Brussels, Belgium

This is explained by the fact that solutions with concentration >50 wt% in H_2O_2 necessitate special attention regarding their storage and transportation and are extremely hazardous.

In that context, on-site or even portable production units to deliver H_2O_2 on-demand could represent an interesting solution to the issues mentioned above, especially for applications that require small amount of highly concentrated product, such as in microelectronics or medical cares. These new perspectives have put again at the forefront of research the direct synthesis of H_2O_2 using microfluidics technology (Inoue et al. 2010). One of the crucial steps in this microfluidic process is to obtain, after reaction, concentrated H_2O_2 by separating it from the other liquid components present in the synthesis process.

Different microfluidic approaches are used for separation (Ciceri et al. 2014; Ziane and Salmon 2015; Ziane et al. 2015). Distillation and pervaporation in microfluidics were already investigated for other systems using different types of set-up (Wootton and de Mello 2004; Hartman et al. 2009; Boyd et al. 2008). Zhang et al. (2010) designed a multi-layered microchip for vacuum distillation of H_2O -MeOH mixtures. The design of the microchip presented in this paper also allows the generation of a temperature gradient along the device, but it is based on a set-up more similar to what Lam et al. (2011) have undertaken. In their microfluidic set-up for multistage distillation of acetone- H_2O mixtures, one side of the chip is heated up, as the other one is cooled down. Separation of acetone from water was also lately investigated in a microfluidic device using PDMS membrane (Zhang et al. 2016). Other examples recently published use PDMS membrane pervaporation process in microfluidic channel for solidification of material (Laval et al. 2016) or to extract the solvent of a dilute colloidal dispersion (Ziane and Salmon 2015). More exotic designs of microchip have been realized for fine distillation. For instance, a rotating spiral microchannel has been used by MacInnes et al. (2010) to take advantage of the centrifugal force to preserve phase separation into parallel-flowing liquid and vapour layers. Microdistillation devices can also be used to dissociate thermodynamically unstable species such as sulphurous acid (Ju et al. 2012).

Regarding the production of H_2O_2 in microfluidics via direct synthesis, we foresee that next attempt will involve the use of MeOH as a co-solvent (with H_2O), essentially because gases (H_2 and O_2) dissolve better in MeOH than in water and because it is inert with the other components. This should increase the concentration of reactants in solution and therefore lead to the production of solution with higher content of H_2O_2 even though will require additional separation step after reaction: H_2O_2 and H_2O will have to be separated from MeOH.

In a previous paper (Ziemecka et al. 2015), we presented the proof of concept that a microfluidic chip based on vacuum pervaporation can be used to separate, at least to some extent, MeOH from the other components of a liquid MeOH- H_2O_2 - H_2O mixture. In the present paper, we further analyse the capabilities of this concept and extend it to purge gas pervaporation. For both vacuum and purge gas configurations, we propose and validate experimentally an original method for the optimization of such a microfluidic chip, while unravelling the key physicochemical phenomena governing its operation. The method is developed for the MeOH- H_2O_2 - H_2O mixture, but could easily be translated to other binary or ternary mixtures.

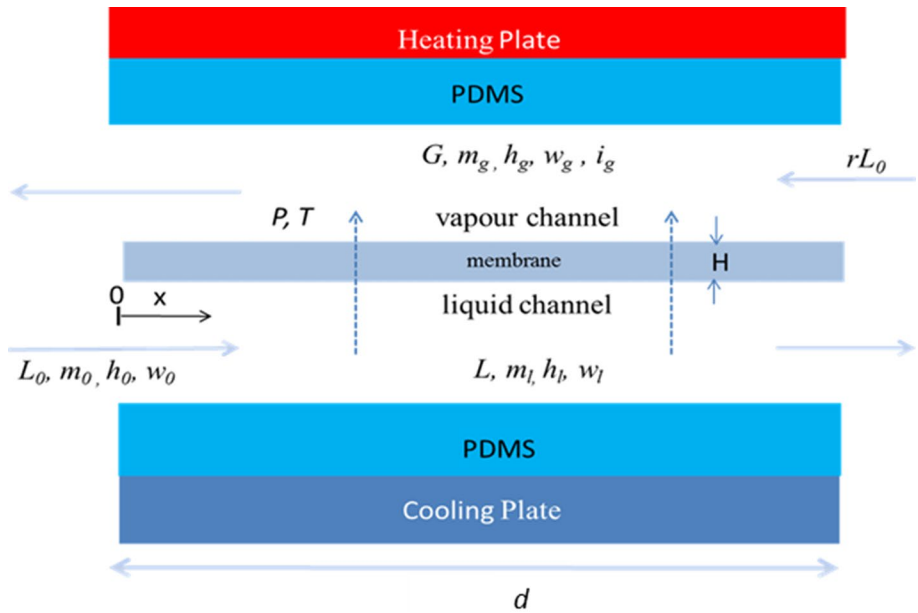
We present in Sect. 2 a dimensionless mathematical model of our microfluidic chip that we solved numerically for screening a wide range of values of the operating parameters for both purge gas and vacuum pervaporation. The operating conditions leading to the best efficiencies of the chip are then identified. The design of the microfluidic chip and the experimental set-up are presented in Sect. 3. The permeability coefficients of the home-made membrane used for the pervaporation were determined experimentally and are provided in Sect. 4. We verify the consistency of the model with experimental results in Sect. 5 and then demonstrate that the high efficiencies predicted by the model could indeed be reached experimentally. Conclusions are presented in Sect. 6.

2 Mathematical model of the separation operation

2.1 Model

The scheme of the operation for the separation of the most volatile compound of a liquid ternary mixture from the other components is described in Fig. 1. This operation is based on the difference in boiling temperature of the three components of the mixture and their abilities of permeating through a dense PDMS membrane. As the liquid permeates by diffusion through the dense membrane, it corresponds to the pervaporation process, which has to be distinguished from the membrane distillation process in which the membrane is only permeable to gases and not liquids. As it will be shown in Sect. 4, this membrane is furthermore not selective to any of the components of the ternary liquid mixture that is considered in this work. Table 1 reports all notations used in this paper. The temperature of the liquid in contact with the membrane is written T , while the pressure in the vapour channel is written P . The liquid feeding mixture is introduced in the cooled part of the chip, in the so-called liquid channel. The inlet molar flow rate of the liquid is written L_0 . The liquid mixture, and purportedly the most volatile component, i.e. MeOH in our

Fig. 1 Scheme of the separation operation



case, pervaporates through the membrane to the heated part of the chip, in the so-called vapour channel. An axis x is defined, with $x = 0$ at the liquid inlet and $x = d$ at the liquid outlet. $L(x)$ is the molar flow rate at position x in the liquid channel, while $G(x)$ is the molar flow rate at position x in the vapour channel. Counter-current flow is realized (i.e. the gas phase outlet is at $x = 0$, while a possible gas inlet is at $x = d$), as we have shown in Ziemecka et al. (2015) that it enhances the performance as compared to a co-current flow. Two configurations are considered: vacuum pervaporation with $G(d) = 0$ and purge gas pervaporation $G(d) = rL_0$, where r is the ratio between the inert gas and the liquid inlet flow rates. We denote $y_0, y_l(x)$ and $y_g(x)$ are the molar fraction of a component in the liquid feeding solution, at position x in the liquid channel and at position x in the vapour channel, respectively, with $y = w$ for water, $y = m$ for methanol, $y = h$ for hydrogen peroxide and $y = i$ for inert gas, which is chosen to be nitrogen in this work.

In our previous paper (Ziemecka et al. 2015), we have developed a mathematical model for the separation operation. In this model, both channels are considered as ideal plug flow reactors. This assumption can easily be verified by checking that, for both channels, the characteristic time of mixing in a cross section of the flow is small compared to the residence time in the channel, while the Bodenstein number of the flow is large compared to unity. In the model, the molar flux density of a component across the membrane is locally calculated as being proportional to the difference between the partial pressure of this component in a gas phase that would be at the equilibrium with the liquid phase (calculated using Raoult's law) and the partial pressure of the component in the vapour channel. The proportionality coefficient is the permeability of the membrane to

this component divided by the thickness of the membrane, noted H hereafter.

Before discussing the behaviour of the operation, we first recast this 1D mathematical model, making the variables and parameters dimensionless as follow,

$$\bar{L} = \frac{L}{L_0}, \quad \bar{G} = \frac{G}{L_0}, \quad \bar{x} = \frac{x}{d}, \tag{1}$$

such that the balance equations composing the model become

$$\frac{d(y_l \bar{L})}{d\bar{x}} = -B(y_l \bar{P}_{sat,y} - y_g \bar{P}), \quad \text{for } y = m, h, w, \tag{2}$$

$$\frac{d(y_g \bar{G})}{d\bar{x}} = sB(y_l \bar{P}_{sat,y} - y_g \bar{P}), \quad \text{for } y = m, h, w, \tag{3}$$

$$\frac{d(i_g \bar{G})}{d\bar{x}} = 0, \tag{4}$$

$$w_l + m_l + h_l = 1, \tag{5}$$

$$w_g + m_g + h_g + i_g = 1, \tag{6}$$

where $\bar{P} = P/P_{atm}$ is the dimensionless pressure in the vapour channel, with P_{atm} the atmospheric pressure, taken equal to 101,325 Pa. $\bar{P}_{sat,y}$ are the dimensionless saturation pressures, calculated using the following equations (Taillet et al. 2013; David 1986; Manatt and Manatt 2004):

$$\bar{P}_{sat,w}(T) = e^{13.7 - \frac{5120}{T+273.15}}, \tag{7}$$

$$\bar{P}_{sat,m}(T) = \frac{1}{P_{atm}} 133 \times 10^{8.8 - \frac{2002}{T+273.15}}, \tag{8}$$

$$\bar{P}_{\text{sat},h}(T) = \frac{1}{760} 10^{44.576 - \frac{4025}{T+273.15} - 12.996 \log^{T+273.15} + 0.004605(T+273.15)}. \quad (9)$$

In Eqs. (2) and (3), B is a dimensionless parameter, given by:

$$B = \frac{WdP_y P_{\text{atm}}}{HL_0}, \quad (10)$$

where W is the width of the liquid channel and P_y is the permeability coefficient of the membrane, which is assumed to be the same for the three components of the liquid mixture and independent of the temperature. These assumptions are justified in Sect. 4. The dimensionless permeability B , also known as the mass Stanton number (Bird et al. 2007), expresses the ratio between the characteristic residence time of the mixture in the liquid channel and the characteristic time of transfer through the membrane.

The dimensionless system is closed with the following boundary conditions:

$$\bar{L}(0) = 1, \quad \bar{G}(1) = r, \quad m_l(0) = m_0, \quad h_l(0) = h_0, \\ m_g(1) = h_g(1) = \epsilon, \quad i_g(1) = 1 - 3\epsilon,$$

where ϵ is the residual molar fraction of each component at $\bar{x} = 1$ in the vapour channel; ϵ should be different from zero to avoid singularities. In practice, $\epsilon = 10^{-6}$ has been found to be small enough for the results to be independent on this parameter, and hence chosen for all calculations. Note that an algebraic expression for i_g can easily be obtained by integrating (4),

$$i_g = r \frac{1 - 3\epsilon}{\bar{G}}. \quad (11)$$

Using (11), the remaining algebraic-differential system of 8 equations is solved as a boundary value problem using the continuation software AUTO-07p (Doedel 2007). The parameter $s = -1$ in Eq. (3) corresponds to the case of a counter-current system as considered here, while the co-current system would correspond to $s = 1$. A trick for solving the counter-current case, since the software AUTO needs a starting solution, has been to calculate a solution for $s = 1$ (co-current) with Mathematica and then continuing the branch of solutions for s going from 1 to -1 , consequently to the counter-current situation. In order to ease the numerical resolution of the equations, they are always solved with $r \neq 0$. It is shown that the solution of the equations is almost independent of r when it is smaller than 10^{-5} , provided that pressure is below a certain value depending on the liquid mixture composition and the operating temperature. Therefore, in practice, vacuum pervaporation can be simulated by using $r \leq 10^{-5}$.

2.2 Parametric analysis

In order to analyse the best conditions of the separation process described above, we define the following efficiencies,

$$\eta_m = 1 - \bar{L}(1) \frac{m_l(1)}{m_0}, \quad (12)$$

$$\eta_h = \bar{L}(1) \frac{h_l(1)}{h_0}, \quad (13)$$

$$\eta = \eta_m \eta_h, \quad (14)$$

where η_m quantifies the ability of the system to extract the methanol from the liquid channel, while η_h quantifies the conservation of H_2O_2 in the liquid channel. Finally, η represents the overall efficiency of the chip. The goal of the separation operation is to obtain a value of η as close as possible to unity. It would mean that the methanol is entirely removed from the liquid phase, while the hydrogen peroxide is entirely kept in the liquid phase. The process enhancement thus aims at obtaining efficiencies as close as possible to unity by properly choosing the operating conditions for a given composition of the feeding mixture, i.e. h_0 and m_0 . As shown in Zhang et al. (2010), some of these operating conditions are involved in the expression of the parameter B , such as the geometry of the chip (length and width of the channels), the thickness of the membrane, the flow rate of the inlet mixture and the permeability of the membrane. The other operating parameters are the temperature of the liquid in contact with the membrane (T), the pressure in the vapour channel (P) and the parameter r in the case of purge gas pervaporation.

In Fig. 2, η_m , η_h and η are presented as functions of B , for different values of r (vacuum pervaporation corresponds to the limit $\eta \leq 10^{-5}$), and for $T = 70^\circ\text{C}$, $P = 0.5$ bar, $m_0 = 0.74$ and $h_0 = 0.11$. The chosen concentration corresponds to a realistic H_2O_2 molar fraction in a liquid that would come out of a microreactor for the production of H_2O_2 , as found, for instance, in the paper of Inoue et al. (2010). It can be observed that η_m increases with an increase in B and with an increase in r . This behaviour is expected according to the definition of B , and as purging gas increases the driving force for the pervaporation, the other parameters hold unchanged. Furthermore, η_m strongly increases when B is increased from 0.1 to approximately 10. Then, for larger values of B , η_m reaches a plateau, corresponding to gas-liquid equilibrium conditions at $x = d$. On the contrary, as it might have been expected too, η_h decreases with an increase in B and with an increase in r . A plateau is also reached for values of B larger than 10, for which η_h remains high (>0.9), except for high values of the purge gas flow rate ($r = 1$). This is due to the fact

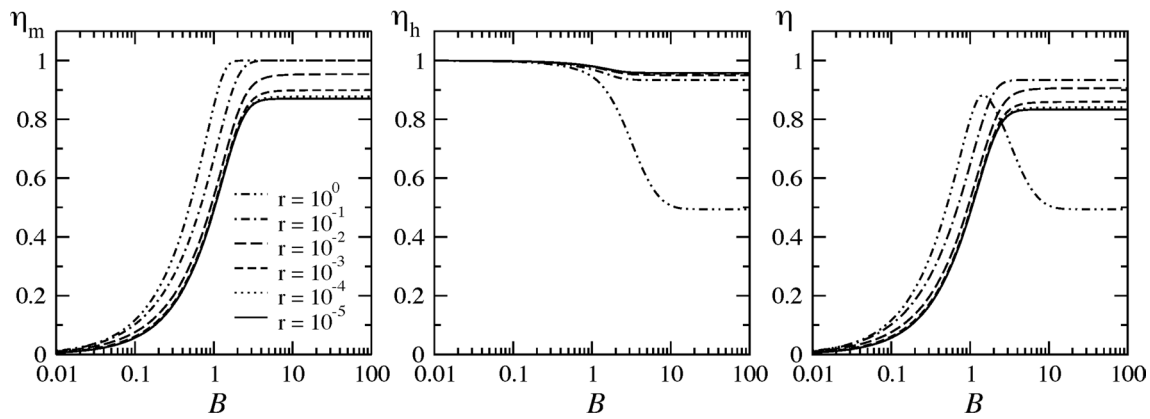


Fig. 2 Efficiencies shown as functions of the parameter B , for different values of the parameter r ; $m_0 = 0.74$, $h_0 = 0.11$, $T = 70$ °C and $P = 0.5$ bar

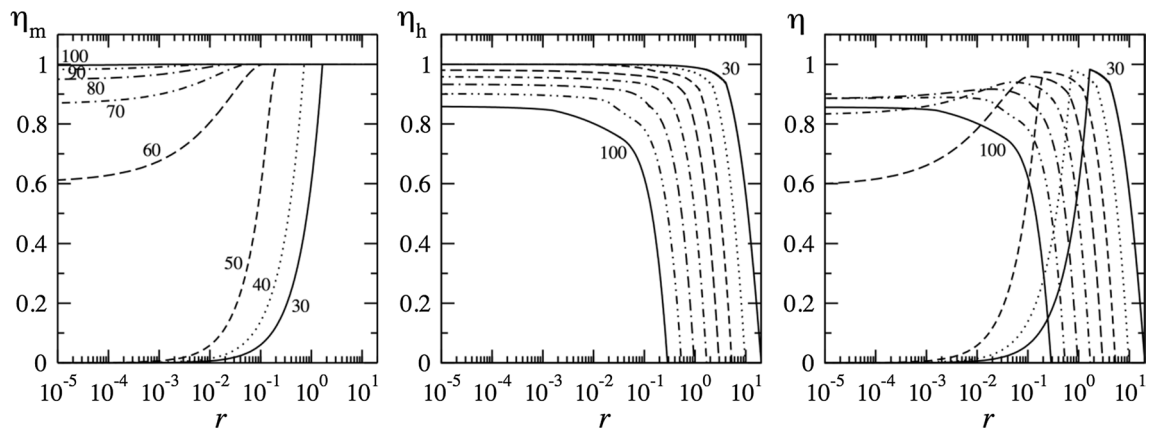


Fig. 3 Efficiencies shown as functions of the parameter r , for different values of T ; $B = 100$, $m_0 = 0.74$, $h_0 = 0.11$ and $P = 0.5$ bar

that the boiling temperature of H_2O_2 is far above the setting temperature 70 °C. Finally, as η_m increases and η_h decreases when B increases, the plot of η versus B should present a maximum. This can easily be observed in Fig. 2 for $r = 1$. This maximum is present for smaller values of r , even though more difficult to observe. Indeed, for $r \ll 1$, η is mainly linked to η_m , as η_h remains close to unity.

As already shown above, remarkably, for large values of B , η becomes independent of B . Consequently, provided we choose a value of B large enough, we can analyse the influence of the other operating parameters on the efficiencies independently of the value of B . The value of $B = 100$ has been found large enough for all the tested conditions and will be used hereafter. Such an analysis is presented in Fig. 3, where η_m , η_h and η are presented as functions of r , for different values of T , with $m_0 = 0.74$, $h_0 = 0.11$ and $P = 0.5$ bar. It can be observed in Fig. 3 that η_m increases with an increase in r and with an increase in T , which is expected as an increase in these two parameters leads to an

increase in the driving force for pervaporation. Therefore, for sufficiently large value of r and/or value of T , $\eta_m = 1$ can be obtained. For the same reasons, η_h decreases with an increase in r and with an increase in T . Interestingly, it appears that η_h is almost constant for small values of r and that, when r becomes larger than a critical value depending on the temperature, η_h suddenly decreases. As a consequence of these observations, the plot of η versus r should presents a maximum as observed in Fig. 3. The abscissa of this maximum depends on the value of T . If the temperature is increased, the value of r at which the maximum efficiency is obtained is decreased. The maximum efficiency of η approaching unity can be obtained at $T = 30$ °C, for $r \approx 2$. In this situation, the temperature in the chip is so far from the boiling temperature of H_2O_2 that almost no H_2O_2 is transferred into the vapour channel. On the other hand, even if the difference between the temperature in the chip and the boiling temperature of the methanol is about 35 °C, the driving force created by the purge gas allows

transferring the entire methanol into the vapour channel. On the contrary, at $T = 100\text{ }^\circ\text{C}$, the maximum efficiency of the chip is obtained for $r \approx 10^{-5}$ corresponding to the regime of vacuum pervaporation. This regime should indeed be considered for large T in order to avoid transferring too much H_2O_2 into the vapour channel. It is noticed that in the regime of vacuum pervaporation, i.e. $r \leq 10^{-5}$, the efficiency η remains below 0.9. Consequently, the maximum efficiencies that can be reached when vacuum pervaporation is used appear smaller than when purge gas pervaporation is used, provided the values of T and P are appropriately chosen.

In order to give more insight into the influence of the operating parameters on the overall efficiency of the chip (η), we present, in Fig. 4, the value of T at which the maximum value of η is reached, as a function of r , for three different inlet mixture compositions and three different values of P , and $B = 100$ to keep the results independent of B . Points in the plane (r, T) corresponding to equal values of η are linked by dotted lines (and the values of η are indicated). It can be observed that very similar trends are obtained for the three different inlet mixture compositions. It is also observed, as mentioned previously, that working at high temperature implies using a small value of r to get an optimal efficiency. On the other hand, working at low temperature implies a high value of r to get an optimal efficiency. High (>0.9) values of η can be reached for a wide range of values of T and r provided P is appropriately adjusted. However, as already mentioned, higher values of the efficiency are obtained in the case of low temperatures and high values of r .

Finally, decreasing P allows using smaller values of T and r to get a same overall efficiency, which could be expected as decreasing the pressure in the vapour channel increases the driving force for the pervaporation.

It is important to recall that the results presented in Figs. 3 and 4 have been obtained using $B = 100$. With such a high value of this parameter, we systematically sit on the plateaus that can be observed in Fig. 2. Hence, the efficiencies become independent of B . Of course, in order to experimentally obtain values of the overall efficiency mentioned in Figs. 3 and 4, the actual value of B , depending on the values of several parameters (the channel length, the membrane permeability, etc.), should be large enough. In Fig. 5, we present the pressure in the vapour channel at which the maximum value of η is reached, as a function of T , for four different values of B , with $m_0 = 0.74$, $h_0 = 0.11$, and $r \leq 10^{-5}$ (vacuum pervaporation). The value of the overall efficiency is also indicated next to each point on this figure. Such a plot is valuable when vacuum pervaporation is preferred (for example due to set-up limitation regarding the introduction of inert gas in the vapour channel). Figure 5 shows that, for $B = 100$, decreasing P leads to an increase in η , if the process is performed at a decreased temperature in order to avoid losing too much H_2O_2 . On the other hand, for $B = 0.1$, the pressure has almost no influence on the optimal efficiency and it is always reached at the same temperature. Consequently, working at low pressure and low temperature cannot be generalized as the best working conditions for vacuum pervaporation because it also depends on the value of B . For $B = 0.1$, η even slightly increases with the pressure.

In Fig. 6, contours of the overall efficiency are presented as a function of P and T , for $m_0 = 0.74$ and $h_0 = 0.11$ and for different couples (B, r) . Figure 6 shows that, for given values of r and B , there is a window of best overall efficiency η in the plane (P, T) . We can observe that an increase in r allows increasing the efficiency of the system while

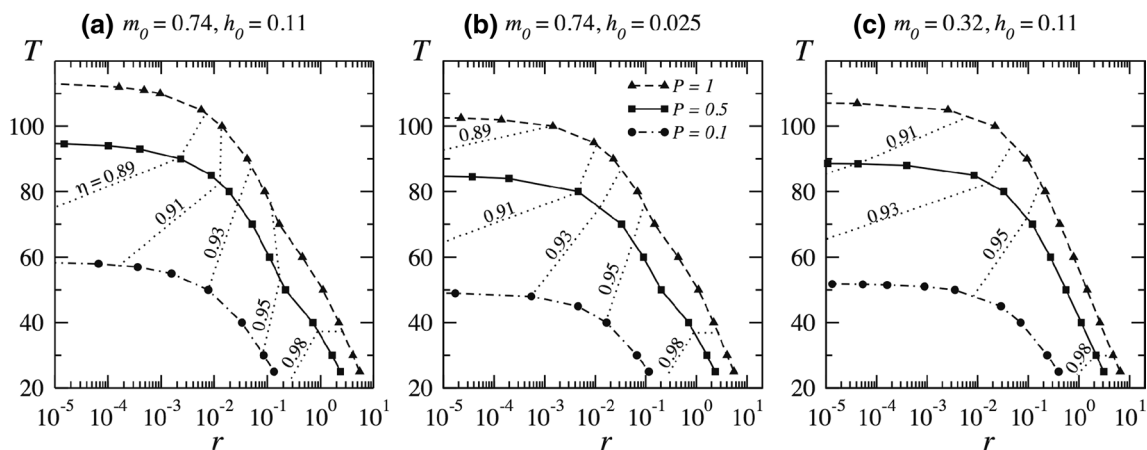
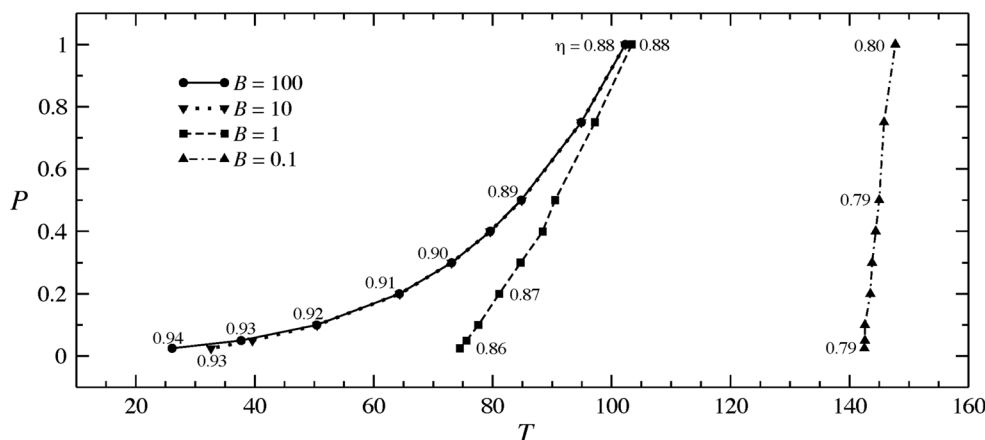


Fig. 4 T at which the maximum value of η is reached, as a function of r , for three different inlet mixture compositions and three different values of P ; $B = 100$ has been used. Points in the plane (r, T) corre-

sponding to equal values of η are linked by *dotted lines* (the values of η are indicated)

Fig. 5 Pressure in the vapour channel at which the maximum value of η is reached, as a function of T , for four different values of B , with $m_0 = 0.74$, $h_0 = 0.11$, and $r \leq 10^{-5}$ (vacuum pervaporation). The value of the overall efficiency is also indicated next to each point on this figure



working at higher pressure (lower partial vacuum). Additionally, increasing the value of B not only allows reaching higher efficiency but also decreases the value of the temperature at which the process should be performed to reach this higher efficiency. However, a decreased pressure is needed to reach this higher efficiency. The empty region on the maps indicates the zone that corresponds to full vaporization of the liquid (and hence a zero overall efficiency).

As a conclusion of this section, we can state that the mathematical model of our microfluidic chip, after validation by experimental results as performed in Sect. 5, can be used to characterize the influence of the operating conditions of the chip on its efficiencies. It allows enhancing the operation of the chip, i.e. within a given set of available operating conditions, selecting the one leading to the maximum overall efficiency. It is shown that, by a fine-tuning of the values of T , P , r and B , a high overall efficiency of the chip could be reached. Of course, it should be checked

that values of T , P , r and B leading to such high efficiencies could indeed be technically achieved, which is also discussed in Sect. 5.

3 Building and operation of the microfluidic chip

3.1 General remarks

A liquid solution of hydrogen peroxide in water (30 wt% in H_2O_2) and liquid MeOH (HPLC grade) were purchased from Sigma-Aldrich. Hexamethyldisilazane was purchased from Fluka Analytical. They were used as received. A liquid solution of hydrogen peroxide in water (60 wt% in H_2O_2) was received from Solvay Company. Polydimethylsiloxane (PDMS) was prepared from Sylgard 184, Dow Corning.

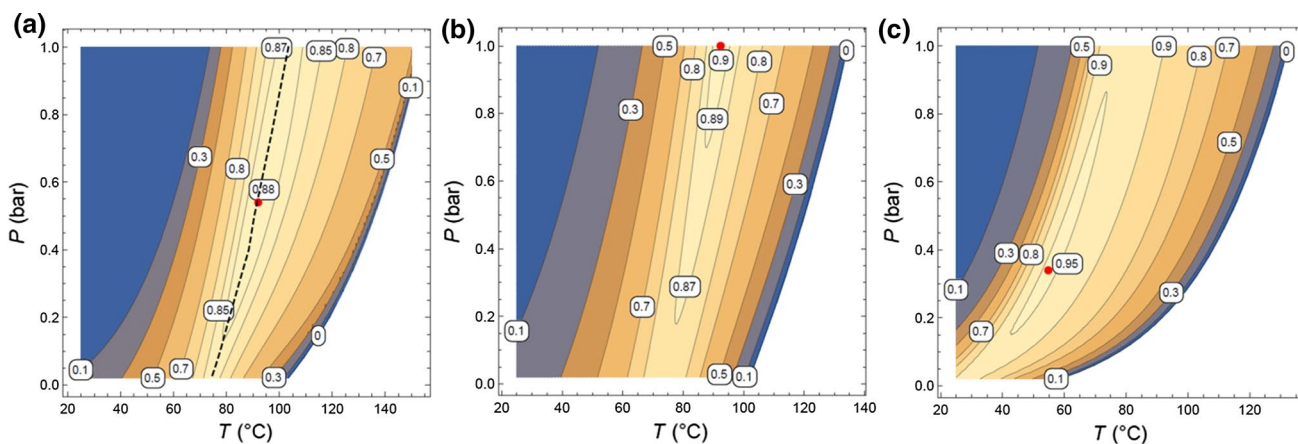


Fig. 6 Contours plots of the overall efficiency as a function of P and T , for $m_0 = 0.74$ and $h_0 = 0.11$. **a** $B = 1$, $r = 10^{-5}$ (vacuum pervaporation), the dashed line is the same as in Fig. 5, **b** $B = 1$,

$r = 0.1$ (purge gas pervaporation) **c** $B = 10$, $r = 0.1$ (purge gas pervaporation). On each figure, the red point represents the optimum value of the efficiency

3.2 Building of the chip

The chips designed for our experiments are built as a multi-layer device as represented in Fig. 7. The key element of this microdevice is a PDMS membrane situated in between two PDMS layers in which the liquid channel and the vapour channel are imprinted. These PDMS layers are in contact with a cooling and a heating device.

3.2.1 Preparation of the microchannels

The soft lithography method is used to fabricate the PDMS layers in which the liquid and vapour channels are imprinted. For this purpose, a photo-resist resin (SU8-2150, MicroChem) is spin-coated on two 4-inch silicon wafers. Then, each of these wafers is exposed to UV light, using the UV-KUB-2 insulator from Kloé Company, through a high-resolution transparency mask containing the 2D design of the liquid or the vapour channel. The non-insulated parts of the resins are subsequently dissolved by dipping the wafers into a bath of SU8-developer. The resulting patterned wafers (by the remaining SU8 structure) are subsequently used as moulds to imprint the liquid and vapour channels in PDMS layers. The liquid channel is 300 μm wide, while the vapour channel is 500 μm wide. The height of both channels is 150 μm . Different channel lengths (0.9 and 2 m) have been used in our experiments.

3.2.2 Preparation of the membrane and of the PDMS layers

The dense membrane is prepared with PDMS (pre-polymer and curing agent in a 5:1, 10:1 or 20:1 ratio by weight). For this purpose, PDMS is spin-coated on a silicon wafer silanized with hexamethyldisilazane and baked at 70 °C for 2 h, for high cross-linking. The resulting membrane thickness (H) was measured by a 3D laser microscopy Keyence VK-X200 at different positions in order to verify the homogeneity. Such a membrane is not selective. The PDMS layers in which the liquid and vapour channel are imprinted are prepared in a similar way, using a mixture of pre-polymer and curing agent in a 5:1 ratio by weight in order to reduce its permeability (see Sect. 4).

3.2.3 Assembly of the chips

Our microfluidic devices are built up from layers of PDMS (the middle one being the membrane). The layers are bonded after 2-min exposure in a plasma chamber (CUTE Femto Science). First, the layer with the liquid

channel is bonded to the membrane. Next, the layer with the vapour channel is bonded to the other side of the membrane, such that the 500- μm -width vapour channel overlaps the 300- μm -width liquid channel. Then, silica wafers with a diameter of 5 cm are placed on both sides of the chip, such that they cover the channels. PDMS (mixture of pre-polymer and curing agent in a 5:1 ratio by weight) is poured on the silica wafers and cured in order to fix the silica wafers. Thanks to the presence of the silica wafers, the chip is less permeable to the gases, and pressure as low as 150 mbar can be reached inside the vapour channel.

3.2.4 Temperature control

A Peltier element (Thermo Electric Modul TES1 12703S, 27 Watt, 14,5 V, BTS Europe BV) is used as a cooling system. The cold side of the Peltier element is directly put in contact with the bottom side of the chip (see Fig. 7). To dissipate the heat, the hot side of the Peltier element is glued to an aluminum plate itself connected to a water-cooling system. A heating resistor (24 V, 40 Watt, 14.5 Ω , GBR-666/24/1, TELPOD) is used as a heating device. It is glued to an aluminium plate itself in contact with the top side of the chip (see Fig. 7). The heating plate is positioned on top of the vapour channel such that condensation of the vapour does not occur within the channel. It also ensures an efficient temperature gradient through the chip due to the cooling plate located underneath the liquid channel. It is noticed that both temperature elements are only covering the serpentine (see Fig. 7). In order to compare experimental results with modelling results, the value of the temperature at the level of the membrane (liquid side) should be controlled. This is realized by measuring precisely the temperature inside the chip with the use of 0.25-mm-diameter thermocouples (Omega, TJ36-CASS-010G-12). The thermocouples are placed at different locations along the liquid and vapour channels. No temperature gradient along the channels is observed, at least within the error of the thermocouples (± 1 °C). The temperature difference between the liquid channel and the vapour channel was measured to be 2 °C for the range of temperatures considered. There can be some inaccuracy in the determination of the temperature in the channels, since the thermocouples are not exactly inside the channels and also since the thermocouple diameter is 0.25 mm, i.e. larger than the height of the microchannel (0.15 mm).

3.2.5 Chip operation

The liquid mixture is introduced in the liquid channel with a syringe pump NEMESYS, at a flow rate of 3.5 or 6 $\mu\text{L}/\text{min}$. The vapour channel is connected to a vacuum pump

(Fluigent) in order to control the value of P . For the experiments involving purge gas, the nitrogen gas flow is introduced at the inlet of the vapour channel with the help of a pressure controller (Fluigent) in line with a gas flow meter (Bronkhorst). Each of the experiments is performed during a few hours in order to collect sufficient amounts of liquid and condensed vapour at the outlets of the chip.

3.2.6 Quantitative analysis

The composition of the output phases of the chip is measured by NMR (Ziemecka et al. 2015). NMR analyses are performed using a 600-MHz Varian instrument. For the measurements, 10 μL of the extracted solution is diluted in 590 μL of acetone- d_6 and measurements are taken at $-25\text{ }^\circ\text{C}$. With these conditions, a good separation of the signals inherent to H_2O_2 , H_2O and MeOH is obtained for our samples, and the concentration can be obtained with the accuracy of 5%.

4 Permeability coefficient measurements

As presented in the Sect. 2 of this paper, the permeability coefficient of a dense membrane is defined, for a given component, as the ratio of the molar flux density of this

component through the membrane, divided by the driving force for this transfer and multiplied by the membrane thickness. This driving force is expressed as the difference between the partial pressure of the component in a gas that would be at the equilibrium with the liquid phase on one side of the channel (this pressure being evaluated by Raoult's law in the model) and the partial pressure of the component in the gas phase on the other side of the membrane.

In order to determine the permeability coefficients of MeOH and H_2O through PDMS membranes, experiments using the chips designed for this work have been realized. The liquid and vapour channels had a length of 0.9 m. The chip was operated with $P = 400\text{ mbar}$, without purge gas, fed with either pure methanol or pure water at a flow rate of 6 $\mu\text{L}/\text{min}$. Three chips with three different membranes were tested for pre-polymer and curing agent in a 5:1, 10:1 or 20:1 ratio by weight. These three different membranes had the same thickness ($H = 100\text{ }\mu\text{m}$). By measuring the liquid and vapour flow rates at the outlet of the chip, the molar flux density across the membrane of the chip could be determined. Then, the permeability of the considered component, P_y ($y = m, w$), was calculated using the following equation:

$$P_y = \frac{HJ_y}{(P_{\text{atm}}\bar{P}_{\text{sat},y}(T) - P)}, \tag{15}$$

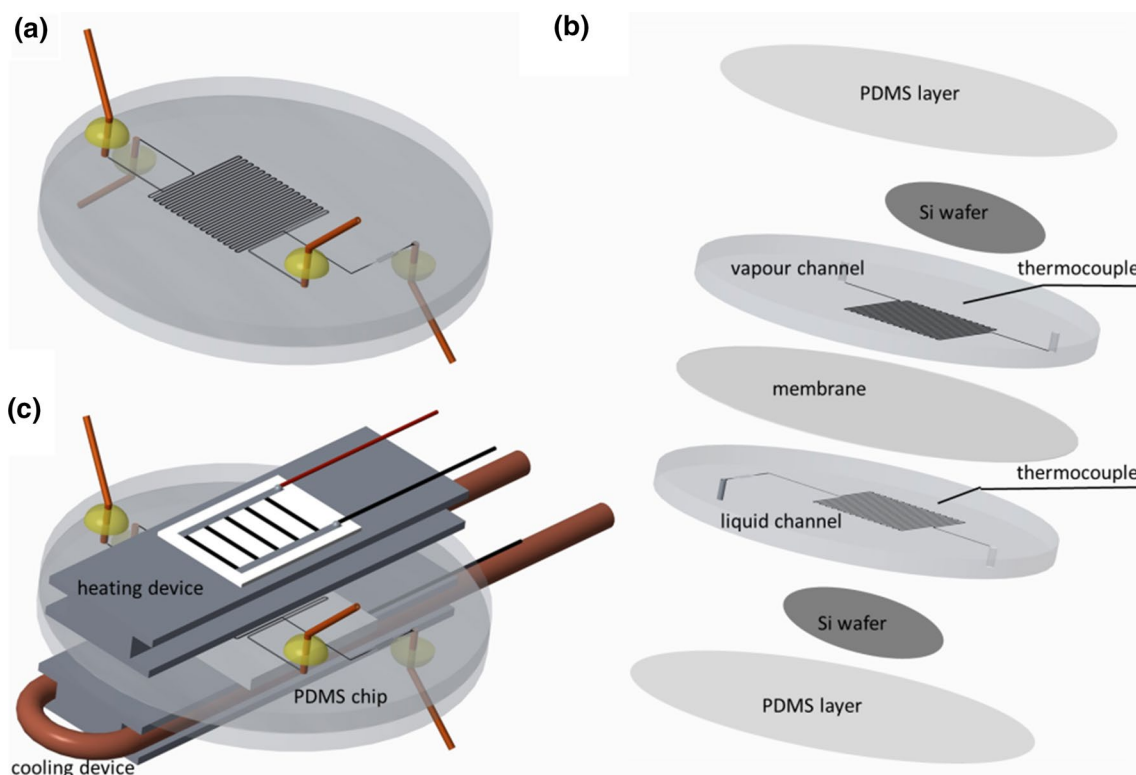
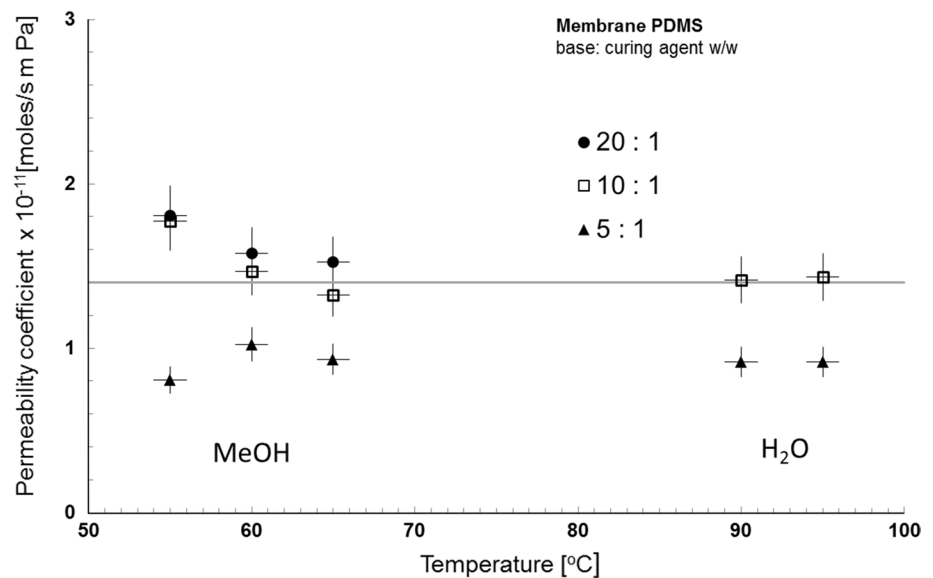


Fig. 7 Scheme of the microfluidic chip: **a** perspective view showing alignment of vapour and liquid channels, **b** assembling of the layers, **c** positioning of the temperature control system

Fig. 8 Permeability coefficients of MeOH and H₂O through three different PDMS membranes, as functions of the temperature inside the liquid channel. The *line* indicates the value from Bell et al. (1988)



where J_y is the molar flux density (mol/s/m^2) of the considered component through the membrane and $\bar{P}_{\text{sat},y}$ is the dimensionless saturation pressure of the considered component.

The experiments were performed for temperature in the liquid channel equal to 55, 60 and 65 °C, when considering MeOH, and equal to 90 and 95 °C, when considering H₂O. The results are shown in Fig. 8. The experiments were performed for three different membranes. They all had the same thickness (100 μm) but different base-to-curing agent ratio. This influences their level of cross-linking and their mechanical properties (Mata et al. 2005). The membrane made with the pre-polymer and the curing agent in a 20:1 ratio by weight is the weakest one and does not mechanically withstand the experimental conditions to determine the permeability coefficient of H₂O at 90 and 95 °C. That is why these data are missing on Fig. 8.

It can be observed in Fig. 8 that the permeability coefficients of MeOH and H₂O are close to each other (i.e. the membrane is non-selective), and almost independent of the temperature. On the other hand, the permeability coefficients appear to depend on the membrane composition. An increased amount of curing agent in the membrane leads to a decrease in the permeability coefficient. The membrane (10:1) is further used in our work because the permeability coefficient of the membrane (5:1) is lower than the permeability coefficient of the membrane (10:1) and because the mechanical properties of the membrane (20:1) are not satisfactory. Therefore, according to the results presented in Fig. 8, when, in the next section, our mathematical model is compared to experimental results obtained with our chips, $P_w = P_m = 1.4 \cdot 10^{-11}$ mol/(m s Pa), independently of the temperature.

According to Bell et al. (1988), P_w and P_m are, for a PDMS membrane at ambient temperature, close to $1.4 \cdot 10^{-11}$ mol/(m s Pa). This value is close to the values obtained with our experiments. However, Bell et al. (1988) did not provide information about the preparation of their PDMS membrane.

Due to the high temperature or low pressure needed, it is impossible to realize similar experiments in order to determine the permeability coefficient of H₂O₂ through the PDMS membranes. Therefore, $P_h = P_m = P_w$ has been assumed to generate the modelling results presented in the next section.

5 Comparison between the model and experimental results

In order to validate our model and to see whether high efficiencies can be reached experimentally, two set of experiments were realized: one using vacuum pervaporation and one using purge gas pervaporation, according to the values of parameters given in Table 2.

A first set of experiments was realized using vacuum pervaporation (no introduction of an inert gas in the vapour channel). The composition of the liquid mixture introduced in the chip was $m_0 = 0.712$ and $h_0 = 0.112$. The flow rate of this liquid was 6 $\mu\text{L}/\text{min}$. The channel had a length of 0.9 m. The corresponding value of the parameter B defined previously is 0.79. According to the modelling results presented in Fig. 5 (that have been generated for approximately the same composition of the inlet liquid and for vacuum pervaporation), this value of B should not allow to reach the maximum value of the overall efficiency that could be reached for an inlet liquid with this composition,

Table 1 Table of notations

List of symbols	
Roman symbols	
B	—Dimensionless parameter, mass Stanton number
d	—Length of the channel (m)
G	—Molar flow rate in the vapour channel (mol/s)
h	—Hydrogen peroxide molar fraction
H	—Thickness of the membrane (μm)
i	—Inert gas molar fraction
J_y	—Molar flux density of the component y (mol/s/m ²)
L	—Molar flow rate in the liquid channel (mol/s)
m	—Methanol molar fraction
P	—Pressure (bar)
P_y	—Permeability coefficient of the component (mol/m s Pa)
Q	—Liquid flow rate ($\mu\text{L}/\text{min}$)
r	—Ratio between the inert gas molar flow rate and the liquid inlet molar flow rate
T	—Temperature ($^{\circ}\text{C}$)
W	—Width of channel (μm)
w	—Water molar fraction
x	—Coordinate along the liquid channel (m)
y	—Molar fraction of the component y ($=m, h, w, i$)
Greek symbols	
ϵ	—Residual molar fraction of each component at the inlet of the vapour channel
η	—Efficiency
Subscripts	
0	—At the inlet
g	—Gas phase
l	—Liquid phase
sat	—Saturation
atm	—Atmospheric
h	—Hydrogen peroxide
i	—Inert gas
m	—Methanol
w	—Water

when vacuum pervaporation is used (η approximately equal to 0.94). The purpose of this first set of experiments is therefore mainly to validate our model (it is worth recalling that the highest efficiencies are obtained when using purge gas pervaporation). The experiments were realized for T between 50 and 81 $^{\circ}\text{C}$ and for P between 0.15 and 0.7 bars. The maximum value of the temperature was selected in order to prevent the thermal decomposition of H_2O_2 (Ziemecka et al. 2015). The minimal value of the pressure was selected according to the technical limitations of our setup. In Fig. 9, the experimental results are compared with the modelling results. The three efficiencies are reported as functions of P and T . A very good agreement between the model and the experimental results can be observed. The

Table 2 Values of the parameters used in both vacuum pervaporation and purge gas pervaporation experiments

	Vacuum pervaporation	Purge gas pervaporation
W (μm) ^a	213 \pm 10	280.5 \pm 10
d (m)	0.9	2
P_y (mol/msPa)	1.4 \times 10 ⁻¹¹	1.4 \times 10 ⁻¹¹
H (μm)	120 \pm 10	100 \pm 10
Q ($\mu\text{L}/\text{min}$)	6	3.5
m_0	0.71	0.71
h_0	0.112	0.112
L_0 (mol/s)	2.82 \times 10 ⁻⁶	1.645 \times 10 ⁻⁶
r	10 ⁻⁵	0.2–0.6
P (bar)	0.15–0.7	1
B	0.79	4.84

^a W is the width of the liquid channel overlapped by the vapour channel

maximum overall efficiency that has been reached experimentally is 0.79 (Fig. 9-right).

A second set of experiments was realized using purge gas pervaporation. The composition of the liquid mixture introduced in the chip was $m_0 = 0.71$ and $h_0 = 0.112$. The flow rate of this liquid was 3.5 $\mu\text{L}/\text{min}$. The channels had a length of 2 m. The corresponding value of the parameter B defined previously is 4.84. It is higher than when vacuum pervaporation was used, because of the increased length of the channels and because of the decreased liquid flow rate. According to the modelling results presented in Fig. 2 (that have been generated for approximately the same composition of the inlet liquid), we might expect that this value of B could allow reaching values of the overall efficiency close to the maximum value that could be reached for an inlet liquid with this composition. The purpose of this second set of experiments is therefore to validate our model but also to see whether it can be used to enhance the operation of the chip, i.e. within a given set of available operating conditions, to select the one leading to the maximum overall efficiency. The experiments were realized at atmospheric pressure—hence, no vacuum pump was needed—for T between 58 and 80 $^{\circ}\text{C}$ and for r between 0.2 and 0.6. In Fig. 10, the experimental results are compared with the modelling results. The three efficiencies are reported as functions of r and T . A very good agreement between the model and the experimental results can be observed. The maximum overall efficiency that is reached experimentally is 0.94, which has been measured 3 times for reproductibility check. This value is also about the maximum overall efficiency of 0.95 that is predicted by the model. It is worth mentioning that if this overall efficiency is smaller than unity, it is mainly due to the transfer of hydrogen peroxide from the liquid to the vapour channel. For the conditions leading to this maximal

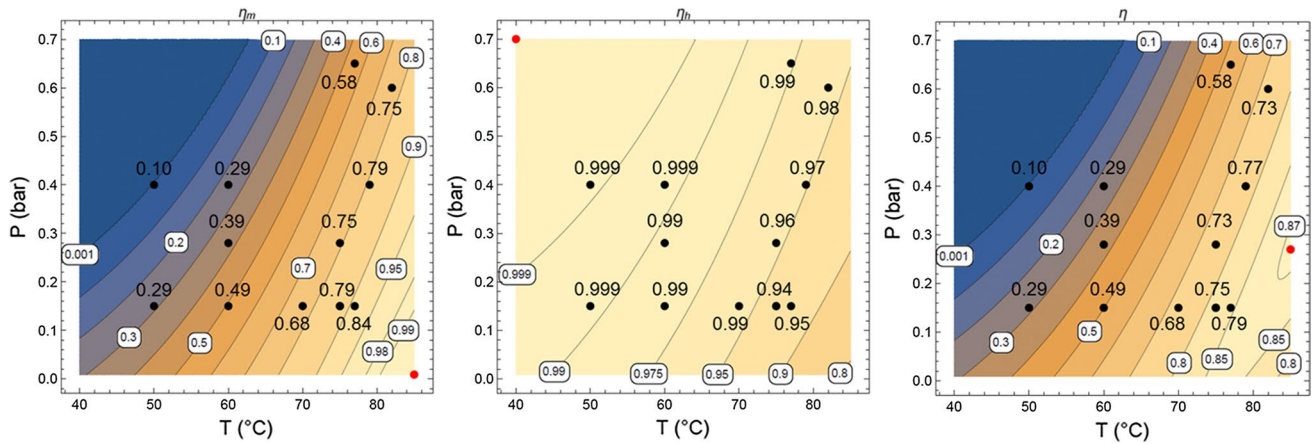


Fig. 9 Efficiencies as functions of T and P . Vacuum pervaporation: $B = 0.79$, $m_0 = 0.712$, $h_0 = 0.112$. The black points give the experimental data

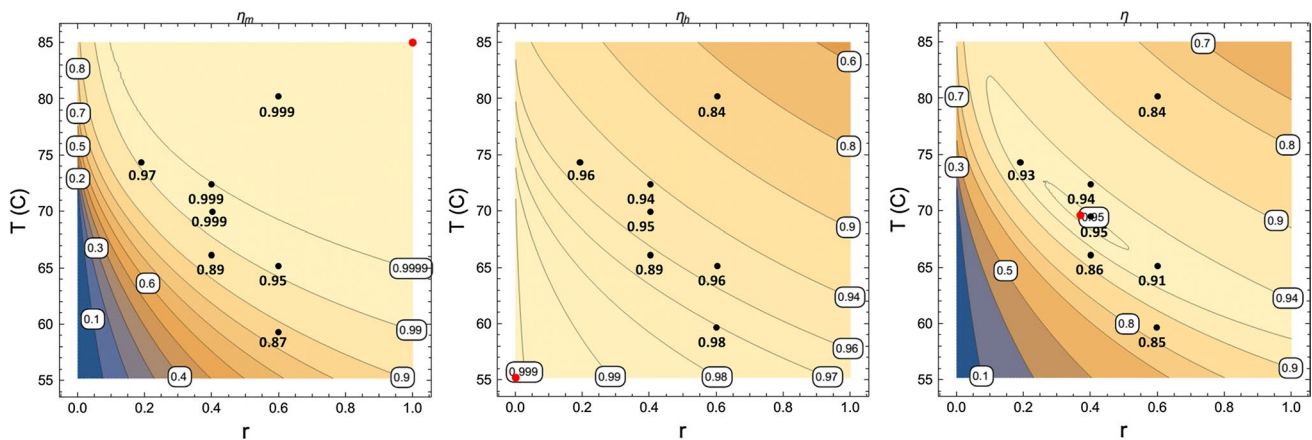


Fig. 10 Efficiencies as functions of T and r . Purge gas pervaporation: $B = 4.84$, $m_0 = 0.71$, $h_0 = 0.112$ and $P = 1$ bar. The black points give the experimental data

overall efficiency, the entire methanol is removed from the liquid. This meets industrial requirement that methanol residue has to be below 1%. At these conditions, hydrogen peroxide concentration is increased by a factor 3 in the liquid phase. Therefore, it is here proven that very high efficiencies can be reached with our chip—even when using atmospheric pressure inside the vapour channel in purge gas mode—and that the model can be used to select the operating conditions leading to the best overall efficiency, within a given set of available operating conditions.

6 Conclusions

A mathematical model allowing a complete parametric study of the separation operation of a ternary mixture was presented, together with an optimization strategy of the

operation for determining the best working conditions for a given set of parameters. The model was experimentally verified for the ternary mixture made of methanol (MeOH), hydrogen peroxide (H_2O_2) and water (H_2O). We defined a dimensionless permeability (B) also referred to as the mass Stanton number, to analyse the behaviour of the system with a minimum number of independent parameters. We also introduced the overall efficiency η that combines the antagonistic effects in the liquid phase of MeOH removal and H_2O_2 retention. From the mathematical model, it is then observed that this efficiency becomes independent of the parameter B for sufficiently large values of B , typically $B \gg 1$, meaning that the liquid/vapour equilibrium has been reached before the outlet of the liquid microchannel. Within that limit, the purge gas-to-liquid flow rate ratio (r) at which the maximum efficiency is obtained decreases when increasing the temperature and/or decreasing the

pressure. Consequently, same efficiencies can be reached at different working conditions, although the highest efficiency in the system, namely 0.98, was obtained for the highest pressure, the lowest temperature and the highest ratio r . Therefore, and as a general rule, higher efficiencies can be obtained with purge gas pervaporation than with vacuum pervaporation. In practical conditions, however, conditions for $B \gg 1$ are barely reachable because of the limitations of the experimental set-up such that the highest possible efficiency strongly depends on the maximum length and width of the channel, maximum membrane permeability, minimum thickness of the membrane and minimum liquid flow rate that can be obtained. Although the method was developed for a specific mixture, it can easily be transposed to other binary, non-ideal or ternary mixtures under the conditions that saturation pressures for used temperatures are known. Even though the flow rate of few $\mu\text{L}/\text{min}$ presented in our system is too small for direct industrial implementation, our system can easily be numbered up by use of replicated parallel chips such as it handles industrially realistic throughput.

Acknowledgements We acknowledge Ir. Hugo Serrano Latorre for Fig. 7, Dr. Pierre Miquel for helpful discussions, Prof. Michel Luhmer for access to the NMR and Hervé Baudine for technical support. We thank the Solvay Company for its input in this project and the Brussels and Walloon regions for the financial support through the WBGreen-MicroEco project. B.S. thanks the F.R.S.-FNRS for financial support as well as BELSPO through the IAP 7/38-MicroMAST project.

References

- Bell C-M, Gerber FJ, Strathmann H (1988) Selection of polymers for pervaporation membranes. *J Membr Sci* 36:315–329
- Bird RB, Stewart WE, Lightfoot EN (2007) *Transport Phenomena*. Wiley, New York
- Bloomfield S, Dhaese PM (2013) Plant for hydrogen peroxide production and process using it, WO2013135491 A1. <https://google.com/patents/WO2013135491A1?cl=no>
- Boyd DA, Adleman JR, Goodwin DG, Psaltis D (2008) Chemical separations by bubble-assisted interphase mass-transfer. *Anal Chem* 80:2452–2456
- Ciceri D, Perera JM, Stevens GW (2014) The use of microfluidic devices in solvent extraction. *J Chem Technol Biotechnol* 89:771–786
- David RL (1986) *Handbook of chemistry and physics*, 67th edn. CRC Press, London
- Doedel EJ (2007) *Auto07p continuation and bifurcation software for ordinary differential equations*, Montreal Concordia University
- Hartman RL, Sahoo HR, Yen BC, Jensen KF (2009) Distillation in microchemical systems using capillary forces and segmented flow. *Lab Chip* 9:1843–1849
- Inoue T, Kikutani Y, Hamakawa S, Mawatari K, Mizukami F, Kitamori T (2010) Reactor design optimization for direct synthesis of hydrogen peroxide. *Chem Eng J* 160:909–914
- Ju WJ, Fu LM, Yang RJ, Lee CL (2012) Distillation and detection of SO₂ using a microfluidic chip. *Lab Chip* 12:622–626
- Lam KF, Cao E, Sorensen E, Gavriilidis A (2011) Development of multistage distillation in a microfluidic chip. *Lab Chip* 11:1311–1317
- Laval C, Bouchaudy A, Salmon J-B (2016) Fabrication of microscale materials with programmable composition gradients. *Lab Chip* 16:1234–1242
- MacInnes JM, Ortiz-Osorio J, Jordan PJ, Priestman GH, Allen RWK (2010) Experimental demonstration of rotating spiral microchannel distillation. *Chem Eng J* 159:159–169
- Manatt SL, Manatt MRR (2004) On the analyses of mixture vapor pressure data: the hydrogen peroxide/water system and its excess thermodynamic functions. *Chem Eur J* 10:6540–6557
- Mata A, Fleischman AJ, Roy S (2005) Characterization of polydimethylsiloxane (PDMS) properties for biomedical micro/nano-systems. *Biomed Microdevices* 7:281–293
- Taillet R, Febvre P, Villain L (2013) *Dictionnaire de physique*, 3rd edn
- Wootton RCR, de Mello AJ (2004) Continuous laminar evaporation: micron-scale distillation. *Chem Commun* 3:266–267
- Zhang YP, Kato S, Anazawa T (2010) Vacuum membrane distillation by microchip with temperature gradient. *Lab Chip* 10:899–908
- Zhang Y, Benes NE, Lammertink RGH (2016) Performance study of pervaporation in a microfluidic system for the removal of acetone from water. *Chem Eng J* 284:1342–1347
- Ziane N, Salmon J-B (2015) Solidification of a charged colloidal dispersion investigated using microfluidic pervaporation. *Langmuir* 31:7943–7952
- Ziane N, Guirardel M, Leng J, Salmon J-B (2015) Drying with no concentration gradient in large microfluidic droplets. *Soft Matter* 11:3637–3642
- Ziemecka I, Haut B, Scheid B (2015) Hydrogen peroxide concentration by pervaporation of a ternary liquid solution in microfluidics. *Lab Chip* 15:504–511